

# Search for a possible quasi-periodic structure based on data of the SDSS DR12 LOWZ

A. I. Ryabinkov, A. D. Kaminker

*Ioffe Institute, Politekhnicheskaya 26, 194021 St. Petersburg, Russia*  
*e-mail: ryabin60@gmail.com, kam.astro@mail.ioffe.ru*

Accepted 2022 xxxx. Received 2022 xxxx; in original form 2022 xxxx

## ABSTRACT

We carry out a statistical analysis of the spatial distribution of galaxies at cosmological redshifts  $0.16 \leq z \leq 0.47$  based on the SDSS DR12 LOWZ catalogue. Our aim is to search and study possible large-scale quasi-regular structures embedded in the *cosmic web*. We calculate projections of the Cartesian galaxy coordinates on different axes (directions) densely covering certain regions in the sky to look for special directions along which one-dimensional distributions of the projections contain significant quasi-periodic components. These components appear as peaks in the power spectra and lie in a narrow range of wave numbers  $0.05 < k < 0.07$ . Particular attention is paid to the evaluation of the significance of the peaks. It is found that the significance of the dominant peaks for some selected directions exceeds  $(4 - 5)\sigma$ . In order to reduce possible selection effects, we create a mock homogeneous catalogue of spatial distribution of galaxies by adding a random set of artificial objects (points) to the real galaxies under study. The power spectrum of this cumulative model data also demonstrates significant peak corresponding to approximately the same scale. As a result we assume the existence of an anisotropic cosmological quasi-periodic structure with characteristic scale  $(116 \pm 10) h^{-1}$  Mpc.

**Key words:** methods:statistical – galaxies: distances and redshifts – cosmology: observations – large-scale structure of Universe

## 1 INTRODUCTION

There are observational evidences in literature (e.g. Saar et al. 2002, Einasto 2014 and references therein) that some domains of the spatial distribution of cosmologically distant objects show elements of spatial regularity with a rather wide range of large scales  $(110 - 140) h^{-1}$  Mpc. Such traces of regularity can be scattered at random locations in a network formed by galaxies, galaxy clusters and superclusters representing both high-density regions – walls, filaments and nodes, and low-density regions – giant voids, occupying the bulk of the space in the Universe (for review see, e.g. van de Weygaert & Schaap 2009, Einasto 2014, van de Weygaert 2016).

Mention can be made here of the deep  $[z \sim (0.1 - 0.4)]$  pencil-beam surveys of galaxies in the direction of the North and South galactic poles produced by Broadhurst et al. (1990) and continued by Szalay et al. (1991), Szalay et al. (1993) and Koo et al. (1993), which showed that the 1D distribution of galaxies may exhibit quasi-periodic components with characteristic scale  $\sim 130 h^{-1}$  Mpc. The heated discussion in the literature about the significance and meaning of these results lasted for more than a decade. Kaiser & Peacock (1991) showed that the quasi-regularity found in the pencil-beam galaxy samples can be explained within the assumption of a random arrangement of galaxy clumps. Only much later, simulations carried

out by Yoshida et al. (2001), taking into account the most probable cosmological models, showed that the probability of a random origin of the detected quasi-regularity can be quite small (less than  $10^{-3}$ ). That indirectly confirmed the quite noticeable significance of the discussed quasi-regularity, but the issue is still open.

The conjecture about the existence of traces of regularity in the distribution of galaxies was supported by an analysis of Landy et al. (1996), based on the Las Campanas Redshift Survey data (at  $z \lesssim 0.1$ ). They plotted 2D Fourier transforms of the galaxy distributions in six thin slices, three in each the North and South Galactic hemispheres, and found significant peaks in certain directions of the wave vector  $\mathbf{k}$  in the 2D power spectra. The peaks correspond to quasi-periods of  $\sim 100 h^{-1}$  Mpc.

An important advancement of the hypothesis of regularity in the distribution of cosmologically distant objects were the works of J. Einasto and co-authors (e.g. Einasto et al. 1994, 1997a,b,c,d, and Einasto et al. 2016, see also Kerscher 1998). It was shown that the cosmological network formed by rich galaxy clusters and superclusters and voids between them may show traces of a regular spatial (cubic-like or shell-like) structure, with characteristic scales  $(115 - 140) h^{-1}$  Mpc.

Somewhat later Saar et al. (2002) proposed a new method for determining quasi-regularity of a cubic-like lattice formed by a network of superclusters and voids. It was shown that a significant

arXiv:2309.12146v1 [astro-ph.CO] 21 Sep 2023

quasi-periodicity with a characteristic scales  $(120 - 140) h^{-1}$  Mpc can be observed along certain directions in space.

Additionally, Einasto et al. (2011a), Einasto et al. (2011b), and Einasto et al. (2019) (also references therein) considered the effects of spatial phases synchronization related to perturbations in different spatial scales and their impact on the formation of the observed cosmic web. It seems to us that such effects of phase ordering can give additional motivation to the search for traces of regularity on larger scales.

In the present work, we try to find further confirmations of this hypothesis, but here we consider much larger redshifts ( $0.16 \leq z \leq 0.47$ ) than it was performed in the works cited above. We focus on studying the spatial distribution of galaxies in the northern hemisphere based on the data of SDSS DR12 LOWZ catalogue (e.g. Dawson et al. 2013, Reid et al. 2016). In our statistical analysis we use methods, which in a sense can be attributed to methods of integral geometry, and combine them with calculations of the power spectra of the obtained distributions.

It is appropriate to mention that methods of integral geometry, in particular the method of Minkowski functionals (e.g. Kerscher et al. 1997, Sahni et al. 1998, Kerscher 2000, Mecke 2000, Appleby et al. 2022), have been widely used to study the morphology and structure of cosmologically distant matter in the Universe during a few past decades. In our case we use the so called *Radon transform* (e.g. Deans 2007, Starck et al. 2005) and some of its modification (see Sect. 5) to look for traces of regularity and anisotropy in the spatial distribution of galaxies. The methods used are not fully integral since they retain selected directions in comoving 3D space on which all the Cartesian coordinates of the galaxies belonging to a sample are projected (integrated). As a result, a one-dimensional distribution of projections of the Cartesian coordinates of galaxies is constructed for any fixed direction  $X$  and then the 1D power spectrum of this distribution is calculated. This procedure allows to determine those directions in space in which a significant quasi-periodicity can be detected. The method turns out to be quite sensitive to very weak traces of ordering in the large-scale structure.

In our previous papers (e.g. Ryabinkov et al. 2013, Ryabinkov & Kaminker 2014, Ryabinkov & Kaminker 2019, hereafter Paper I, Ryabinkov & Kaminker 2021, hereafter Paper II) we analysed mainly the so called *radial distributions* of cosmological objects (the luminous red galaxies, LRGs, or the brightest cluster galaxies, BCGs), which can be imagined as homogeneous spherical shells filled with the objects depending only on the comoving distance from the center of spherical system, while the angular coordinates of the objects are completely ignored. In these papers, the power spectra of the radial distributions  $P_R(k)$  were calculated and significance levels of peaks in the region  $k \sim (0.05 - 0.07) h \text{ Mpc}^{-1}$  were estimated in some way or another. So in Paper I the method to assess the significance of the peaks was proposed based on the exponential distribution of peak amplitudes (see Eq. (5)) with taking into account dependences of  $\langle P_R(k) \rangle$  on  $k$ , where  $\langle \dots \rangle$  is averaging over the ensemble of realizations. It was shown, in particular, that  $\langle P_R(k) \rangle$  for extremely large ensembles of radial distributions constructed with respect to various centers scattered over the homogeneous space tends to be equal to 3D power spectrum  $P_{3D}(k)$  averaged over various directions of wave vector  $\mathbf{k}$ . Using the method proposed in Paper I, the results of Ryabinkov et al. (2013) and Ryabinkov & Kaminker (2014) were reevaluated and it turned out that the significance of the peaks in the radial power spectra obtained in these articles did not exceed  $3\sigma$  level contrary to the estimates made in these works.

In Paper II on the basis of several samples extracted from the

SDSS DR7 catalogue by Kazin et al. (2010) we considered the radial distributions of the LRGs, within an interval  $0.16 \leq z \leq 0.47$ , restricted by rectangular regions (*sectors*) in the sky. It was shown that the radial distributions in some selected sectors characterized by certain directions contain significant ( $\gtrsim 4 - 5 \sigma$ ) quasi-periodic components with the same periods ( $\gtrsim 110 h^{-1}$  Mpc) as the values received in Ryabinkov et al. (2013) and Ryabinkov & Kaminker (2014) for a much wider view of the sky. Perhaps this indicated the anisotropy of the quasi-regular structure distributed over a certain spatial region.

Also in Paper II we proposed to apply the Radon transform and subsequent calculations of 1D power spectra for searching the direction of the maximum peak amplitude. For various samples under consideration it was found that there is quite a narrow bunch of directions exhibiting significant quasi-periodicities with close periods  $116 \pm 10 h^{-1}$  Mpc. Such directions are characterized by the angular coordinates of the Equatorial coordinate system clustering around right ascensions  $\alpha_0 \simeq 175^\circ \pm 2^\circ$  and declinations  $\delta_0 \simeq 25^\circ \pm 2^\circ$ . In addition, in Paper II we carried out preliminary calculations based on the extended SDSS DR12 data in a wider range ( $0.16 \leq z \leq 0.72$ ) and obtained confirmation of the possible existence of an anisotropic quasi-regular structure with the same characteristic scale.

In the present study we confirm our previous conclusions about the possible existence of a weak (i.e. manifested by the integral methods mentioned above) anisotropic quasi-periodic structure in the spatial distribution of galaxies. Moreover, we find approximately the same specific direction of the  $X$ -axis, the projection onto which the Cartesian coordinates of galaxies contains a quasi-periodic component corresponding to the highest level of significance ( $\gtrsim 4 - 5\sigma$ ). These findings encourage us to continue similar statistical analysis on larger samples beyond the SDSS data. The first very preliminary experience with catalogs of photometric data is represented in Sect. 7.

In Sect. 2 we describe the observational data, employed in this work. In Sect. 3 we determine basic quantities and definitions used in further analysis. In Sect. 4 we employ the Cartesian coordinate system (CS) and introduce the Radon transform with its subsequent 1D power spectrum calculations. In Sect. 5 we introduce and apply another technique, the so-called oriented cuboids method. In Sect. 6 we show that the sample of the LOWZ galaxies within the interval  $0.16 \leq z \leq 0.4$  in the strict sense is not homogeneous (not volume-limited) and build (somewhat artificially) a model homogeneous sample. Conclusions and discussions of the results are given in Sect. 7.

## 2 DATA USED

In the present consideration we use data on galaxies with redshifts  $0.16 \leq z \leq 0.47$  from the SDSS DR12 (LOWZ and CMASS) catalogues accumulated only for the northern hemisphere in the sky and represented in three data files:

*galaxy\_DR12v5\_LOWZ\_North.fits.gz*,

*galaxy\_DR12v5\_CMASSLOWZE3\_North.fits.gz*

*galaxy\_DR12v5\_CMASS\_North.fits.gz*,

which are available in the Science Archive Server.<sup>1</sup> A description of the catalogues of the DR12 can be found, e.g. in Dawson et al. (2013), Alam et al. (2015), Reid et al. (2016).

<sup>1</sup> <https://data.sdss3.org/sas/dr12/boss/lss/>

We restrict ourselves mainly by spectroscopic data on redshifts (with exceptions in Sect. 6 and partly in Sect. 7) with redshift uncertainty  $\Delta z/(1+z) \sim 5 \times 10^{-4}$  (see, e.g. Bolton et al. 2012), which provide a reliable determination of heterogeneity, both irregular and regular, in the considered scales. However, our first experience in the statistical analysis of galaxy cluster catalogues (e.g. Wen et al. 2012 and Wen & Han 2022) with photometric redshifts, determined with uncertainty  $\sim (0.01 - 0.02)$  at  $z \lesssim 0.5$ , confirmed to some extent the findings obtained from the spectral data. This will be discussed briefly in the Sect. 7.

The SDSS DR12 LOWZ region is shown in Fig. 1 in the Equatorial coordinates mainly in the northern hemisphere (marked in grey). Our basic sample includes galaxies, falling into a large rectangle region delineated by thick dashed lines. This helps to avoid possible effects of the irregular edges on the borders of the entire grey area. We choose the same intervals of the right ascension  $140^\circ \leq \alpha \leq 230^\circ$  and declination  $0^\circ \leq \delta \leq 60^\circ$  as it was chosen in Paper II for the SDSS DR7 catalogue.

It should be noted that the selected rectangular area includes parts of two gaps (filled in fig. 1, see below) associated with the incompleteness of the sample of galaxies in the LOWZ catalogue. The gaps correspond to earlier observations with a different galaxy selection algorithm (see Reid et al. 2016 for details). Inside a rectangular area the main gap with a missing number of galaxies located within the area in the sky  $185^\circ \lesssim \alpha \leq 230^\circ$  and  $25^\circ \lesssim \delta \lesssim 40^\circ$ ; the second gap at  $\delta \gtrsim 0$  is not statistically significant (Figures 8 and A1 of Reid et al. 2016).

Reid et al. (2016) generated a sample ‘LOWZE3’ including all areas of incompleteness that overlap with the rectangle represented in Fig. 1 (*chunks 3-6* in the terminology of Reid et al. 2016). Mentioned above the CMASS catalogue was combined with the LOWZE3 sample to create the ‘CMASSLOWZE3’ sample which is also available on the DR12 Science Archive Server. To fill the gaps inside the rectangular region and in adjacent areas shaded in solid grey in Fig. 1, we had to extract the ‘LOWZE3’ from the ‘CMASSLOWZE3’ (subtracting the CMASS galaxies) and clear the resulting sample from galaxies which are also present in the LOWZ catalogue. Then we created a new combined sample ‘LOWZ’ + (refined) ‘LOWZE3’ which is shown in Fig. 1.<sup>2</sup> The sample selected in such a way contains 176,962 galaxies detected within the large rectangle in Fig. 1 and the redshift interval indicated above. In Sects. 4 and 5 we briefly discuss that the results obtained turned out to be robust to such (not quite strict) a gap-filling procedure.

Following methodology described in Paper II we scan the selected rectangle region using a mobile trial sector with angular dimensions  $5^\circ$  (right ascension) and  $25^\circ$  (declination). In this way, we select 144 (partly overlapping) sectors for the whole rectangular area. Within each sector we build the so-called radial (1D) distribution function of galaxies  $N_R(D)$ , where  $D$  is defined in Eq. (2),<sup>3</sup> and calculate the 1D radial power spectra  $P_R(k)$  for the distributions.

Thus, six sectors were found in Paper II on the base of SDSS DR7 data, in which the significance of peaks in the radial power spectra within the interval  $0.05 < k < 0.07 h \text{ Mpc}^{-1}$  exceeded  $3\sigma$ . In the present analysis we act differently, we choose a smaller

<sup>2</sup> The sample ‘LOWZ’+‘LOWZE3’ have been also produced by Reid et al. (2016) but the corresponding file is not available in the Science Archive Server indicated above.

<sup>3</sup> The radial (shell-like) distribution function  $N_R(D)$ , averaged over angles  $\alpha$  and  $\delta$  within a selected area (e.g. sector) in the sky, was described and analysed in Papers I and II.

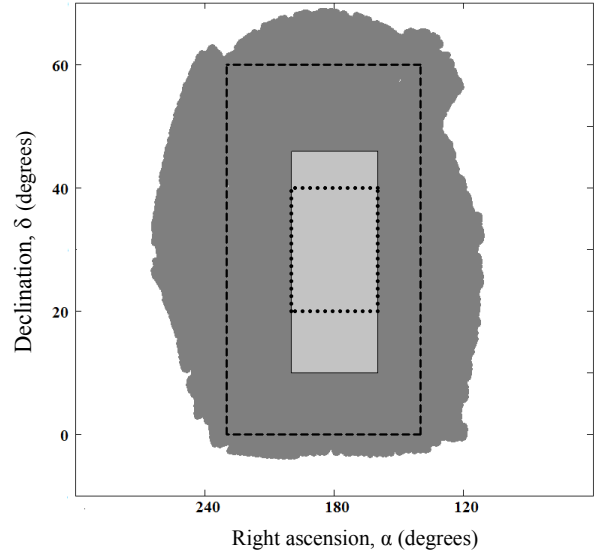


**Figure 1.** (Colour online) Angular distribution of galaxies over the sky from the SDSS DR12 LOWZ data in the Equatorial CS; the entire grey coloured region together with the rectangle included in it (marked in light grey) comprise the LOWZ northern hemisphere sample with a somewhat artificially filled regions (gaps) of data incompleteness (see text); *dashed* lines delineate the general rectangular region of a given statistical consideration with  $140^\circ \leq \alpha \leq 230^\circ$  and  $0^\circ \leq \delta \leq 60^\circ$ ,  $\alpha$  and  $\delta$  are indicated near the coordinate axes ( $\alpha$  is shown in a standard way: west on the right, east on the left). Light grey marks a smaller rectangular region on the celestial sphere,  $160^\circ \leq \alpha \leq 200^\circ$  and  $10^\circ \leq \delta \leq 46^\circ$ , in which the effects considered in the text are especially significant. The dotted lines bound a smaller area of the rotation of  $X$ -axis described in Sect. 4.

rectangular region with  $160^\circ \leq \alpha \leq 200^\circ$  and  $10^\circ \leq \delta \leq 46^\circ$  (marked in light grey in Fig. 1), including three (central) of the six indicated sectors with the highest significance levels of the peaks in the corresponding radial power spectra.

In Sect. 4 (Fig. 2) and in Sect. 6 (Fig. 5) we consider only this (smaller) rectangular area in which we can expect a higher probability to detect traces of quasi-periodicity using the approach described in these sections.

Note that the data of DR12 LOWZ catalog that we use here are not strictly homogeneous [see, e.g. Fig. 5 (a)], so in Sect. 6 we use an extended model sample, specially prepared as homogeneous one. The results turned out to be resistant to such simulations.

### 3 CARTESIAN COORDINATE SYSTEM. BASIC DEFINITIONS

Let us consider spatial distribution of galaxies presented in the DR12 LOWZ catalogue within certain region in the sky using the Cartesian CS:

$$\begin{aligned} X_i &= D(z_i) \sin(90^\circ - \delta_i) \cos \alpha_i \\ Y_i &= D(z_i) \sin(90^\circ - \delta_i) \sin \alpha_i \\ Z_i &= D(z_i) \cos(90^\circ - \delta_i), \end{aligned} \quad (1)$$

where  $D(z_i)$  is radial comoving distance of  $i$ -th galaxies with redshifts  $z_i$ , measured in  $h^{-1} \text{ Mpc}$  (e.g. Kayser et al. 1997; Hogg 1999)

$$D(z_i) = \frac{c}{H_0} \int_0^{z_i} \frac{1}{\sqrt{\Omega_m(1+z)^3 + \Omega_\Lambda}} dz, \quad (2)$$

$H_0 = 100 h \text{ km s}^{-1} \text{ Mpc}^{-1}$  is the present Hubble constant,  $c$  is the speed of light;  $\alpha_i$  – its right ascension and  $\delta_i$  – declination; in both the coordinate systems an observer is at the origin.

Hereafter (for comparison with our previous results), we use the same  $\Lambda$ CDM model with  $\Omega_m = 0.25$  and  $\Omega_\Lambda = 1 - \Omega_m = 0.75$  as it is chosen in Paper II.

Following Paper II we apply the method of constructing 1D distributions of projections of the Cartesian coordinates of galaxies onto different  $X$ -axes rotated relative to each other around the origin. In this approach the basic value for the spectral analysis is an 1D distribution function  $N_X(X)$  collecting all projections of the coordinates within outlined angular region on the fixed  $X$ -axes;  $N_X(X)dX$  is a number of galaxies inside an interval  $dX$ . As in Paper II we use the binning approach<sup>4</sup> and calculate so-called normalized 1D distribution function in the comoving CS as a number of projections of the Cartesian coordinates inside longitudinal non-overlapping bins:

$$\text{NN}(X_c^l) = \frac{N_X(X_c^l) - S_X}{\sqrt{S_X}}, \quad (3)$$

where  $X_c^l$  is a central point of a bin,  $l = 1, 2, \dots, \mathcal{N}_b$  is numeration of bins,  $S_X$  is a mean value of the 1D distribution  $N_X(X_c^l)$  over all bins under study. Essentially, the magnitude of  $\text{NN}(X_c^l)$  can be considered as a function of the signal-to-noise ratio along the selected  $X$ -axis. We use such a representation of Eq. (3) for evaluations in Sect. 7.

The values of  $\text{NN}(X_c^l)$  allows one to calculate corresponding 1D power spectrum

$$P_X(k_m) = |F_X^{1D}(k_m)|^2 = \frac{1}{\mathcal{N}_b} \left\{ \left[ \sum_{l=1}^{\mathcal{N}_b} \text{NN}(X_c^l) \cos(k_m X_c^l) \right]^2 + \left[ \sum_{l=1}^{\mathcal{N}_b} \text{NN}(X_c^l) \sin(k_m X_c^l) \right]^2 \right\}, \quad (4)$$

where  $F_X^{1D}(k_m) = (\mathcal{N}_b)^{-1/2} \sum_{l=1}^{\mathcal{N}_b} \text{NN}(X_c^l) e^{-ik_m X_c^l}$  is the one-dimensional discrete Fourier transform,  $k_m = 2\pi m/L_X$  is a wavenumber corresponding to an integer harmonic number  $m = 1, 2, \dots, \mathcal{M}$ ,  $\mathcal{M} = \lfloor \mathcal{N}_b/2 \rfloor$  is a maximal number (the Nyquist number) of independent discrete harmonics,  $\lfloor x \rfloor$  denotes the greatest integer  $\leq x$ ,  $x$  is an arbitrary real (positive) number;  $L_X$  is the whole interval in the configuration space, i.e. the so-called *sampling length*.

Then we rotate the coordinates  $XYZ$  at the certain Euler angles so that the new  $X'^5$  is oriented in a certain direction ( $\alpha'$  and  $\delta'$ ) relative to the initial Equatorial CS. Performing a sequence of such rotations we search for  $X_0$ -axis or a direction along which the 1D power spectrum displays the most significant peak for  $k$  within the interval  $0.05 < k < 0.07$ .

To control the uniformity of statistics for different directions of  $X$  we fix the same boundaries of the rotated axes  $464 \leq X \leq 1274 h^{-1} \text{ Mpc}$  which contain  $\mathcal{N}_b = 81$  independent bins with a width  $\Delta_X = 10 h^{-1} \text{ Mpc}$ . On the other hand, we limit ourselves

<sup>4</sup> The  $X$ -axis is divided into a finite number of non-overlapping intervals - bins, each of which accumulates a certain amount projections of coordinates of galaxies. Thus the continuous distribution of projections  $N_X(X)$  is replaced by a discrete one  $N_X(X_c^l)$  (see Eq. 3).

<sup>5</sup> Hereafter, denotation  $X'$  instead of general denotation  $X$  indicates the axis  $X$  of the rotating CS.

to such a scanning region of  $X'$  directions that on the boundary of this region all bins  $\Delta_{X'}$  would be filled (more or less evenly) with projections of galaxy coordinates. In addition, we need to make sure that the amplitudes of the peaks of power spectra in the neighborhood of  $k$  indicated above, calculated for borders of this region would be small enough (significance should be  $\lesssim 3\sigma$ ). The latter condition provides us by the background area around the domain with increased peak amplitudes where the peaks are likely to have random nature. Such areas are suitable for assessing the significance of the peaks (see below).

To satisfy these conditions, we restrict the area of analyzed directions of  $X'$  by intervals  $160^\circ \leq \alpha' \leq 200^\circ$  and  $20^\circ \leq \delta' \leq 40^\circ$ , i.e. the smallest rectangle in Fig. 1 bounded by dotted lines.<sup>6</sup>

Actually, here we deal with a discrete analog of the so-called 3D Radon transform (e.g. Deans 2007) applied to selected data in comoving coordinate system, i.e. we summarize the projections of all subsample points, falling into each bin along  $X$ . Thereafter, we exploit two main properties of the Radon transform (i) *translation invariance* that allows one to transfer the projections of the Cartesian coordinates of galaxies on the given  $X$  axis to another  $\hat{X}$  axis parallel to the original one, (ii) *linearity*, which allows one to summarize the projections obtained for individual sectors in the sky in the total sum of projections to get a single Radon transform for the entire sample.

It was verified numerically in Paper I for a set of the power spectra  $P_R(k)$  simulated specially for radial distributions of objects ( Sect. 3 in Paper I) that the cumulative probability function of random peak amplitudes  $P_k$  at any  $k = k_{\text{max}}$  integrated over all values lower than a fixed value  $P_k^*$  can be expressed as (see also, e.g. Bardeen et al. 1986, Feldman et al. 1994)

$$\mathcal{F}(P_k < P_k^*, \lambda) = 1 - \exp(-\lambda \cdot P_k^*) \quad \text{at } P_k^* \geq 0, \quad (5)$$

where  $\lambda = \lambda(k)$  is a parameter of the exponential distribution determined by a reciprocal mean (mathematical expectation) peak amplitude  $M[P_k] = \langle P_R(k) \rangle$ , i.e.  $\lambda(k) = \langle P_R(k) \rangle^{-1}$ . Eq. (5) allows one to obtain significance of a peak in 1D power spectra when it is possible to calculate *ensemble-averaged* or *volume-averaged* amplitudes of spectra at a given  $k$ .

Following Paper II we apply this technique to determine the significance levels of peaks in 1D power spectra  $P_X(k)$  calculated using Eq. (4). This way the significance levels can be found from Eq. (5) assuming that  $\lambda(k) = \langle P_X(k) \rangle^{-1}$ , where  $\langle P_X(k) \rangle$  is an average power spectrum calculated by rotating of the  $X$ -axis within some *background* area in the sky in which no significant peaks ( $\sim 3\sigma$ ) have been found in the interval of  $k$  we are interested in.

Eq. (5) allows us to calculate fixed confidence probabilities for different  $k$  and relate them in by one smooth curve to outline an appropriate significance level over the entire interval under study ( $0 \leq k \leq 0.3$ ). Such curves can be exploited as a measure of significance for spectral peaks obtained at any  $k$ .

## 4 RECTANGLE REGION. RADON TRANSFORM

We start by orienting the  $X$ -axis along the direction with coordinates  $\alpha = 160^\circ$  and  $\delta = 20^\circ$  (lower right corner of the rectangle region in the *left panel* of Fig. 2, coinciding with the smallest rectangle in Fig. 1). We build the 1D distribution of projections on this axis of

<sup>6</sup> Not confuse with the region that provides the analyzed sample of galaxies, i.e. the entire light grey rectangular region in Fig. 1.

all Cartesian coordinates of galaxies falling into the entire light grey rectangular area in Fig. 1 ( $160^\circ \leq \alpha \leq 200^\circ$ ,  $10^\circ \leq \beta \leq 46^\circ$ ) and calculate using Eq. (4) the 1D power spectrum along this direction. Then we rotate sequentially the axis  $X'$  shifting the right ascension or declination with a step  $1^\circ$  and scanning in this way the entire area shown on the left panel of Fig. 2. Such rotations of the moving CS require only two Euler angles,  $\alpha_{Eu} = \Delta\alpha$  and  $\beta_{Eu} = \Delta\delta$ , where  $\Delta\alpha$  and  $\Delta\delta$  are respective rotation angles.

In such a way one can determine the existence of dominant peaks in the power spectra at  $k \sim (0.05 - 0.07) h \text{ Mpc}^{-1}$  for a number of directions  $X'$  and delineate areas of increased significance of the peaks. Likewise one can find an axis  $X_0$  with the Equatorial coordinates  $\alpha_0$  and  $\delta_0$  along which the 1D distribution of the coordinate projections shows the maximum peak height at indicated  $k$ .

The results of our calculations of the cumulative 1D power spectra are represented in Fig. 2. The *left panel* in Fig. 2 shows two confidence areas (two shades of grey) in the sky indicating peak amplitudes (for a scale  $2\pi/k_{\text{max}} = 116 h^{-1} \text{ Mpc}$ ) exceeding the significance levels  $3\sigma$  (light grey) and  $4\sigma$  (grey), respectively. Maximum value of the peak is achieved along the direction of  $X_0$  with coordinates  $\alpha_0 = 171^\circ$  and  $\delta_0 = 26^\circ$  (small white square). Colorless area (“empty” region) corresponds to the absence of peaks in 1D spectra, whose significance reaches  $\sim 3\sigma$ .

The *right panel* represents the power spectrum  $P_X(k)$  calculated for normalized 1D distribution (Eq. 3) of the galaxy coordinate projections on the  $X_0$ -axis with  $\alpha_0$  and  $\delta_0$  indicated above. The dashed line show significance levels evaluated as it is described in Sect. 3 with using Eq. (5). The average 1D *background* power spectra,  $\langle P(k) \rangle$ , calculated by scanning over the left (“empty”) half of the entire *left panel* in Fig. 2, i.e. at  $180^\circ \leq \alpha \leq 200^\circ$  and  $20^\circ \leq \delta \leq 40^\circ$  (total  $21 \times 21 = 441$  power spectra). In this way one can obtain the mean significance level ( $3\sigma$  and  $4\sigma$  in Fig. 2).

However, all power spectra calculated for close  $X$ -axes are correlated (not independent). Therefore, to calculate the mean variance of given significance we use a special procedure of separation of  $X$ -directions within the *background* field. We found that correlations between the power spectra in different  $X$ -directions decrease to values  $< 0.5$  at angles of  $\gtrsim 5^\circ$  between the  $X$ -axes. Thus we select a sample of 16 independent  $X$ -directions each of them is separated by  $5^\circ$  from its nearest neighbors.

Then we build 25 such non-overlapping samples, employing sequential shifts of the entire grid by  $1^\circ$  along  $\alpha$  and/or  $\delta$  axes. Using Eq. (5) and pre-computed average power spectra  $\langle P(k) \rangle$  we calculate a fixed significance level (e.g.  $4\sigma$ ) for each sample (grid) at all considered  $k$  from the entire interval  $0 \leq k \leq 0.3$ . Now we can estimate the variance of 25 smoothed dependences on  $k$  calculated for the fixed level of significance (treating them as random ones for each  $k$ ). The result of such estimations is shown in the right panel of Fig. 2 as the upward expanding band of the  $4\sigma$  significance.

The main feature of these calculations is the use of the 3D Radon transform (e.g. Deans 2007) along the selected axis forming the entire sample of points. The resulting 1D distribution turns out to be sensitive to the presence of rarefied quasi-periodic components in the spatial distribution of galaxies. As a result one can see that the dominant peak in  $P_X(k)$  at  $k = k_{\text{max}}$  reaches the upper edge of the  $4\sigma$  band and has a height (amplitude modulus squared) about 200 (slightly more).

Worth to compare the result shown in Fig. 2 with results of Paper II represented in Fig. 4 (data of the SDSS DR7) and in the right panel of Fig. 7 (black curve; data of the SDSS DR12). The last two indicated figures refer to the galaxies observed through

6 selected narrow sectors belonging to the same large rectangular area as outlined by the dashed lines in Fig. 1. Note that the scanning area by the  $X$ -axis was chosen the same in all compared cases, i.e.  $160^\circ \leq \alpha \leq 200^\circ$  and  $20^\circ \leq \delta \leq 40^\circ$ , as well as the same interval along  $X$  ( $464 \leq X \leq 1274 h^{-1} \text{ Mpc}$ ) was considered, to ensure the same conditions for the Radon transforms in all directions under study.

One can notice that significant peaks in the power spectra were obtained at the same  $k = k_{\text{max}} = 0.054 h \text{ Mpc}^{-1}$  with close directions of the  $X_0$  axis (maximum peak):  $\alpha_0 = 176^\circ$ ,  $\delta_0 = 24^\circ$  for the DR7 catalog and  $\alpha_0 = 175^\circ$ ,  $\delta_0 = 25^\circ$  for the DR12 LOWZ catalog in Paper II. Moreover, the areas of increased significance of the peaks also largely overlap.

It can be seen that the results of this work are well consistent with the results of Paper II, although we use more stringent significance criteria in the present study. Actually, the significance of the peak in the right panel of Fig. 2 does not exceed  $4\sigma$ , while its height is about 200. That is noticeably greater than the height of the considered peaks in Fig. 7 (black curve in the right panel) of Paper II<sup>7</sup> whose significance has been assessed as  $\gtrsim 5\sigma$ .

If we do not carry out the gap filling procedure (described in Sect. 2) in the distribution of galaxies included in the LOWZ catalogue, then we get the same peak in the power spectrum as in the *right panel* of Fig. 2 even with a height of 204.6 (instead of 201.3) at statistics of 48,776 galaxies (instead of 50,972). Thus, the incompleteness of galaxies (see Fig. 8 by Reid et al. 2016) does not affect the main result.

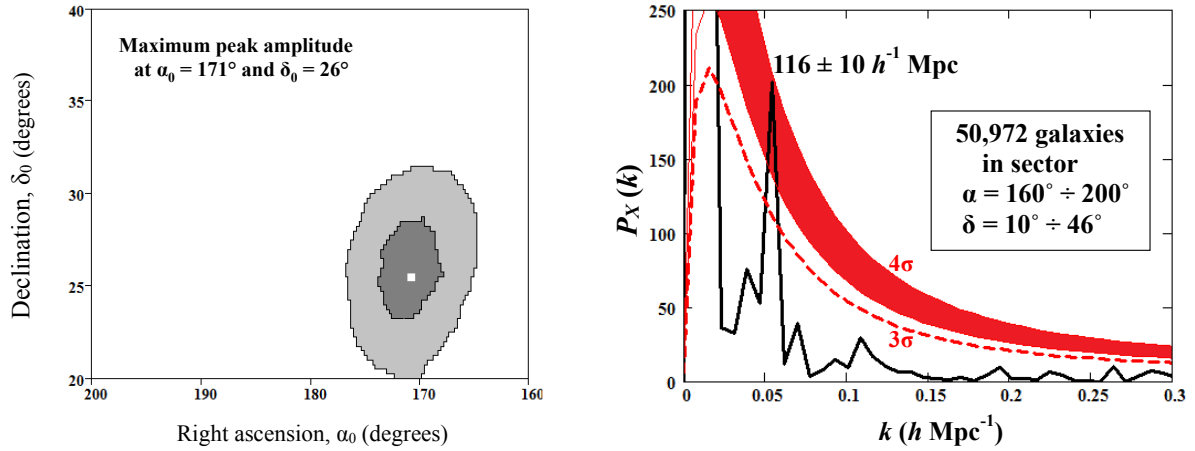
## 5 RECTANGLE REGION. ROTATING CUBOID

Fig. 3 demonstrates results of applying another method of searching for the traces of periodicity in the same scan area of the  $X$ -axis, as in the *left panel* of Fig. 2. For this purpose we build a *cuboid* (rectangular parallelepiped) in space with fixed the Cartesian coordinates  $X, Y, Z$  (see below), the  $X$ -axis being responsible for the orientation of the cuboid in space. We define vertices and faces of the cuboid and calculate the projections of the coordinates of all galaxies from the LOWZ catalog, falling into the cuboid, onto the direction of  $X$ -axis. This direction is determined by the angles  $\alpha$  and  $\delta$  in the Equatorial CS. As in the Sec. 4, we build the 1D distribution of these projections and calculate its power spectrum, then we rotate the  $X$ -axis along with the cuboid around the origin  $X = 0$  and repeat the whole procedure at each step of the cuboid’s rotation.

As the first step, the  $X$ -axis is aligned with the direction of the maximum amplitude of the peak in the power spectra shown in the *left panel* of Fig. 2, i.e.  $\alpha_0 = 171^\circ$  and  $\delta_0 = 26^\circ$ . Then we move the vertices of the cuboid, changing its orientation but without changing its shape and size, until the peak in the power spectrum within the interval  $0.05 < k < 0.07$  reaches the maximum. The coordinates of the vertices and positions of the edges found in this way are indicated in the inset in the *right panel* of Fig. 3. Thus, the positions of the faces closest to the observer and the most distant from him are defined by a condition  $344 \leq X \leq 1274 h^{-1} \text{ Mpc}$ . Let us notice asymmetric shifts of the vertices along the  $Y$ - and  $Z$ -axes relative to the  $X$ -axis ( $-90 \leq Y \leq 480 h^{-1} \text{ Mpc}$ ,  $-300 \leq Z \leq 320 h^{-1} \text{ Mpc}$ ).

The vertex coordinates in the Cartesian CS obtained in this

<sup>7</sup> Mainly because we used extended interval of  $X$  for such assessments in Paper II and different areas in the sky (6 sectors) for the basic sample of galaxies.



**Figure 2.** (Colour online) *Left panel:* areas of fixed confidence levels ( $\beta = 1 - p$ ) of the peaks in 1D power spectra  $P_X(k)$  at  $k_{\max} = 0.054 h \text{ Mpc}^{-1}$  calculated using the Cartesian coordinates of galaxies projected on various axes  $X$  (falling in a fixed range  $464 \leq X \leq 1274 h^{-1} \text{ Mpc}$ ) sequentially rotated relative to each other by  $1^\circ$  within the region  $160^\circ \leq \alpha \leq 200^\circ$  and  $20^\circ \leq \delta \leq 40^\circ$  (bounded by dotted lines in Fig. 1). The marked areas are: light grey  $-\beta = 0.998$  ( $3\sigma$ ), grey  $-\beta = 0.999936$  ( $4\sigma$ ); white square indicates the direction of the maximum peak height  $X_0$  ( $\alpha_0$ ,  $\delta_0$ ). *Right panel:* 1D power spectrum  $P_X(k)$  (solid line) with a maximum peak (at  $k = k_{\max}$ ) calculated for projections of the galaxy coordinates on the  $X_0$ -axis; significance level  $3\sigma$  (dashed line) and a variety of significance levels  $4\sigma$  within the upward expanding band with a width equal to the variance built for 25 separated samples of the *background* power spectra (see text). The inset shows the total sample of studied galaxies and the  $\alpha$ ,  $\delta$  intervals (light grey rectangular region in Fig. 1) including the Equatorial coordinates of all galaxies in this sample; symbol ‘ $\div$ ’ means an interval, e.g.  $\alpha_1 \leq \alpha \leq \alpha_2$ .

way rotating together with the cuboid do not change in the process of scanning by the  $X$ -axis (with a step  $1^\circ$ ) of the entire area  $160^\circ \leq \alpha \leq 200^\circ$  and  $20^\circ \leq \delta \leq 40^\circ$ . For all valid  $X$ -axis orientations and subsequent constructions of cuboids with respect to these directions, the boundaries of the volume of cuboids capture all detected galaxies inside the large rectangle in Fig. 1. This expands the statistics of galaxies compared to Sect. 4. On the other hand, almost all positions of the cuboid (with minor exception) locate within the large rectangle.

The *left panel* of Fig. 3 looks similar to the left panel of Fig. 2. Actually, a highlighted area inside the scanning sector of the  $X$ -axis is quite consistent with the oval-like area in the left panel of Fig. 2. Both areas correspond to the increased significance of peaks in the power spectra with that difference that the *left panel* of Fig. 3 contains a (dark grey) region with significance  $\gtrsim 5\sigma$ , which is missing in Fig. 2. The small white square also indicate the direction of the maximum  $X_0$  ( $\alpha_0 = 170^\circ$ ,  $\delta_0 = 28^\circ$ ) at  $k = k_{\max} = 0.054 h \text{ Mpc}^{-1}$ . This direction is quite close to the direction of the maximum spectral peak obtained for the Radon transforms (Fig. 2).

The *right panel* of Fig. 3 is also organized similar to the right panel in Fig. 2. A very high peak in the 1D power spectra (calculated for the  $X_0$ -direction) with a height  $\sim 300$  at  $k = 0.054 h \text{ Mpc}^{-1}$  is visible. Two significance levels ( $3\sigma$  and  $4\sigma$ ) represented by dashed lines and the wide band corresponding to  $5\sigma$  are also calculated in the same way as it is described in Sec. 4 for  $4\sigma$  level.

The main difference between the two methods is that during rotations of the cuboid there is a partial exchange of galaxies from the general array captured by the cuboid in different positions, while in the approach of Radon transforms we use projections onto different  $X$ -axes (but with fixed boundaries of the interval  $X_1 \leq X \leq X_2$ ) from a single sample of galaxies bounded by a smaller rectangle in Fig. 1. It can be concluded that scanning of the area shown in the *left panel* of Fig. 3 by the  $X$ -axis, accumulating all projections

of galaxy coordinates falling into the cuboid, gives a more efficient way to search for quasi-periodicity in the space distribution of the galaxies. Moreover, it can be assumed that projections of coordinates of galaxies falling into the cuboid onto the  $X_0$ -axis make it possible to roughly localize the spatial regular structure if it is really exists.<sup>8</sup>

Note that comparison with results obtained in a similar way for the unfilled gaps in the LOWZ catalogue, occurring within the large rectangle in Fig. 1, leads to the same conclusion as the one at the end of Sect 4. Indeed, we get the same peak in the power spectrum, as in the *right panel* of Fig. 3, whose height is 297 (instead of 299) with statistics of 67,359 (instead of 70,831).

## 6 HOMOGENEOUS SAMPLE MODELING

Fig. 4 (a) shows the absolute  $g$ -band magnitudes  $M_g$  of the sample of galaxies observed within the largest angular rectangle ( $140^\circ \leq \alpha \leq 230^\circ$ ,  $0^\circ \leq \delta \leq 60^\circ$ ) in Fig. 1 in dependence on the comoving distance  $D(z)$  (Eq. (2)). The rest-frame absolute magnitude of the  $i$ -th galaxy with the redshift  $z_i$  is defined according to Beck et al. (2016) as  $M_{g,i} = m_{g,i} - 25 - 5 \log [(1 + z_i)D(z_i)/(h^{-1}\text{Mpc})] - K_{g,i}(z = 0)$ , where  $m_{g,i}$  is the apparent  $g$ -band magnitude,  $K_{g,i}(z = 0)$  is the corresponding  $K$ -correction.

The considered interval  $464 \leq D \leq 1274 h^{-1} \text{ Mpc}$  corresponds to redshifts  $0.16 \leq z \leq 0.47$ . Each point on the  $(D, M_g)$ -plane represents a galaxy from the DR12 LOWZ catalog. In this section, we neglect the existence of the area of incompleteness in the LOWZ sample (*chunks* 3 – 6 in the notation of Reid et al. 2016) and do not use the gap-filling procedure described in Section 2. The

<sup>8</sup> Note that the Radon transform allows one only to determine the main direction  $X$  of quasi-periodicity, but not its localization in space.

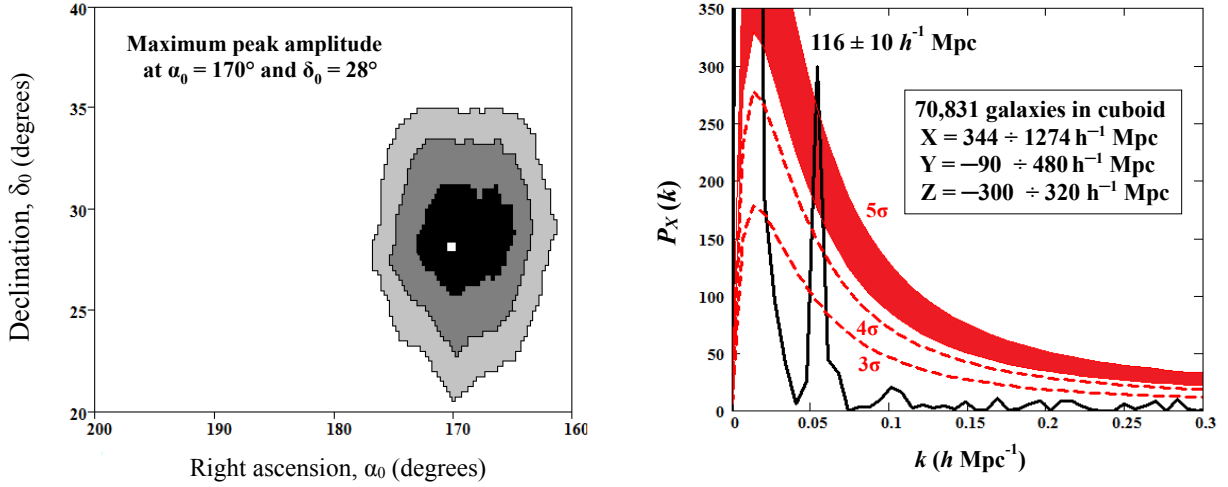


**Figure 3.** (Colour online) Results of similar calculations as in Fig. 2 but produced for the samples of Cartesian coordinates of LOWZ galaxies falling into sequentially rotated cuboid with fixed boundaries of coordinates  $X$ ,  $Y$ ,  $Z$  indicated in the inset on the (right panel). Left panel: areas of the confidence levels similar to the left panel of Fig. 2, but with the addition of  $5\sigma$  significance area ( $\beta = 0.9999994$ , dark grey). The white square also indicates the direction  $X_0$  of the maximum spectral peak height ( $\alpha_0$  and  $\delta_0$ ). Right panel: 1D power spectrum (solid line) with the maximum peak (at  $k = k_{\max} = 0.054 h \text{ Mpc}^{-1}$ ) calculated for the 1D distribution of coordinate projections on  $X_0$ -axis; significance levels  $3\sigma$  and  $4\sigma$  (dashed lines) and the upward expanding band with diversity of significance levels  $5\sigma$  are calculated using power spectra obtained the same way as in Fig. 2. The total number of galaxies falling into the cuboid oriented in the  $X_0$  direction is also indicated in the inset.

results obtained below indicate again that the region of incompleteness does not principally affect the appearing of quasi-regularity traces. The total number of points (sample size) within the interval  $-23.2 \leq M_g \leq -21.2$  is 163,473 galaxies.

The absolute  $g$ -band magnitude  $M_g$  were found in the database SDSS SkyServer (e.g. Beck et al. 2016)<sup>9</sup> <sup>10</sup> using additionally the selection conditions given in the formulas (9 - 12) by Reid et al. (2016), as well as keeping the fixed region of equatorial coordinates and the fixed interval  $z$  (indicated above). Note, however, that the error of such an identification remains rather uncertain.

In order to determine  $M_g$  of analyzed galaxies in the LOWZ catalogue we have created a new table based on the SDSS SkyServer database containing three galaxy identification parameters: two Equatorial coordinates  $\alpha$ ,  $\delta$  and spectroscopic redshifts  $z_s$  and their photometric  $g$ -band absolute magnitudes  $M_g$ . The first three parameters were used to search for the same galaxies in the DR12 LOWZ catalogue (*galaxy\_DR12v5\_LOWZ\_North.fits.gz*) with the subsequent assignment to them of the corresponding  $M_g$ . As a result 163,473 galaxies included in both the lists were selected, and their absolute magnitudes  $M_g$  were found.

In Fig. 4 (a) one can see an inhomogeneous distribution of points with comoving distance  $D$ , in particular, for brighter objects below the  $M_g < -21.8$  (upper dashed line). However, for even brighter  $M_g < -22.2$  (lower dashed line) but rarer galaxies, the visible distribution becomes more homogeneous.

Fig. 4 (b) demonstrates a systematic shift of the  $g$ -band absolute magnitudes  $-23.2 < M_g < -21.8$  between the data of two catalogues of the LRGs DR7 [Full DR7 LRG sample presented by

Kazin et al. (2010)]<sup>11</sup> and DR12 LOWZ catalogue in combination with the database SDSS SkyServer as described above. The figure represents the distribution of the difference between absolute magnitudes of two catalogues related to a sample of the same LRGs, the intervals of the equatorial coordinates ( $\alpha$  and  $\delta$ ) and the comoving distances ( $464 \leq D \leq 1274 h^{-1} \text{ Mpc}$ ) being the same as in the panel (a). Under these conditions, the total number of LRGs common for these two catalogues is 17,680.

The shift  $\Delta M_g \approx 0.4$  represented in Fig. 4 (b) makes it difficult a direct comparison of galaxy distributions falling within the same intervals of  $M_g$  from the DR7 and the DR12 LOWZ catalogues. In particular, the conditions of a volume-limited sample ( $n(D) \approx \text{const}$  or  $n(z) \approx \text{const}$ ) are satisfied for the subsample DR7-Bright presented by Kazin et al. (2010) (at  $-23.3 \leq M_g \leq -21.8$  and  $0.16 \leq z \leq 0.44$ ), but this does not match with the properties of the sample obtained in the present work.

Figs. 4 (c) and (d) illustrate this difference. They show dependences on the comoving distances  $D(z)$  of the LOWZ galaxy number densities  $n(D)$ , averaged over the angular coordinates within the sky region indicated above. Here we use a bin  $\delta D = 1 h^{-1} \text{ Mpc}$  and a smaller interval of  $D(z)$  than in Fig. 4 (a),  $464 \leq D \leq 1000 h^{-1} \text{ Mpc}$  (or  $0.16 \leq z \leq 0.36$ ). The panel (c) corresponds to the absolute magnitudes  $-23.2 < M_g < -21.8$  (17,086 galaxies), while the panel (d) – to the brighter and rarer galaxies at  $-23.2 < M_g < -22.2$  (4251 galaxies). The small bin size turned out to be more suitable to perform linear regression (see below), while the decrease in the upper limit of the interval  $z$  provides almost constant average number density (cf. with Figure 2 of Kazin et al. 2010).

The thick solid lines in both the panels (c) and (d) correspond to the linear regression determined by the maximum likelihood method (e.g. Ledermann & Lloyd 1984)  $n(D) = c_1 + c_2(D - \bar{D})$  with

<sup>9</sup> <http://skyserver.sdss.org/dr12/en/help/docs/realquery.aspx>

<sup>10</sup> The galaxy (photometric) identifier (19-bit number) p.ObjID queried from the basic catalogue of galaxies, *photoprimary p*, allows one to join the requested data on  $\alpha$ ,  $\beta$ ,  $z_s$  in the spectroscopic table, *specphotoall s*, with the data on  $M_g$  in the photometric table *photoz ph*.

<sup>11</sup> <https://cosmo.nyu.edu/~eak306/SDSS-LRG.html>

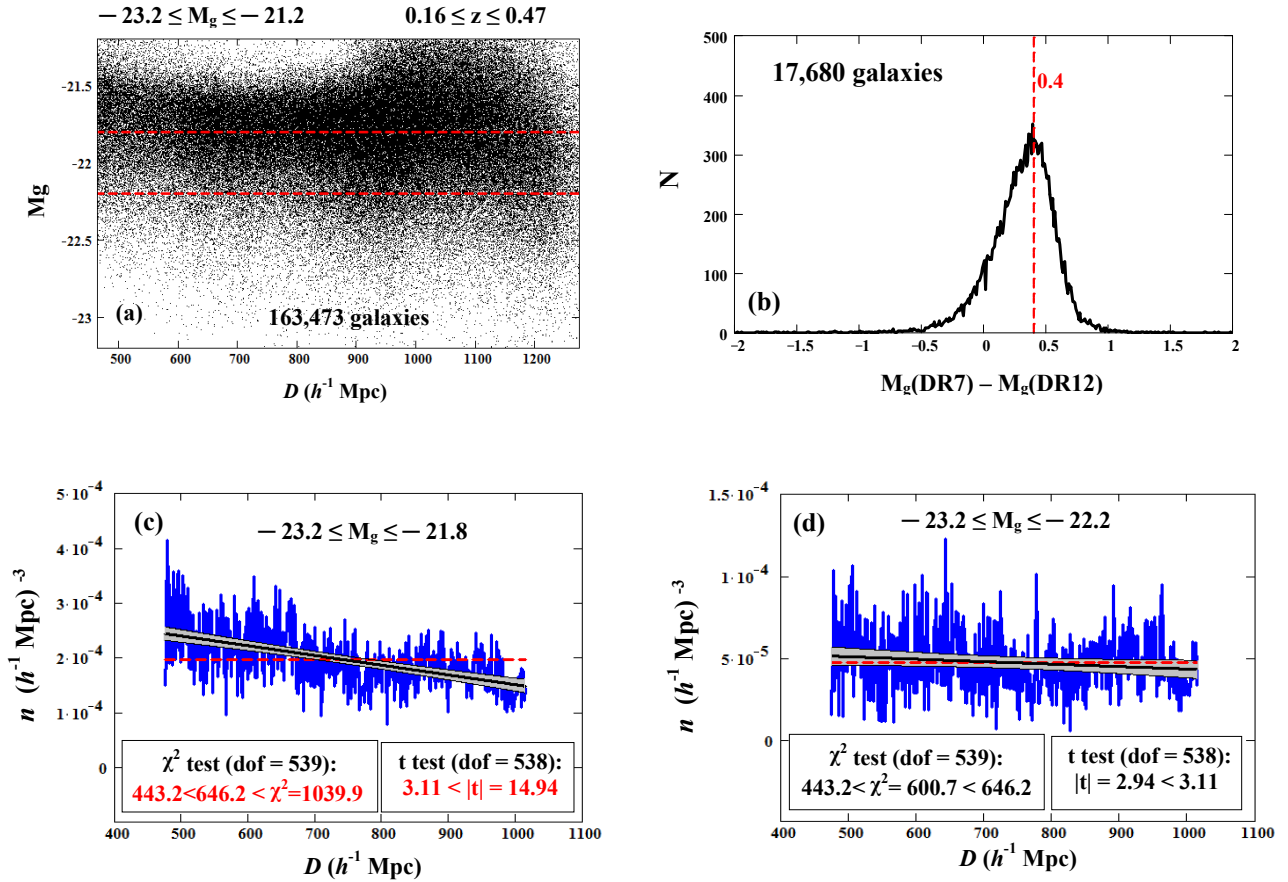


**Figure 4.** (Colour online) *Panel (a)*: distribution of the LOWZ galaxies, observed within the angular rectangle  $140^\circ \leq \alpha \leq 230^\circ$  and  $0^\circ \leq \delta \leq 60^\circ$ , and the interval of redshifts  $0.16 \leq z \leq 0.47$ , on the  $(D(z), M_g)$ -plane, where  $D(z)$  is the comoving distance and  $M_g$  is the absolute  $g$ -band magnitude. Two horizontal dashed lines indicate the levels  $M_g = -21.8$  and  $-22.2$  from top to bottom, respectively. The total number of galaxies included in the distribution is indicated at the bottom. *Panel (b)*: distribution of differences of absolute magnitudes  $M_g(\text{DR7}) - M_g(\text{DR12})$  (on condition  $-23.2 \leq M_g \leq -21.8$ ) of the same galaxies registered in two different catalogues: DR7 and DR12 LOWZ (see text). The intervals of angular coordinates  $\alpha$  and  $\delta$ , and redshifts  $z$  are the same as in the *panel (a)*. The vertical dashed line indicates the maximum of the distribution. The number of galaxies included in the distribution is also shown. *Panel (c)*: average number density  $n(D)$  as a function of the comoving distance on the same condition ( $-23.2 \leq M_g \leq -21.8$ ) as in the *panel (b)* and within the same angular rectangle region as in the *panels (a)* and *(b)*, but for a shorter interval  $464 \leq D \leq 1000 h^{-1} \text{ Mpc}$  ( $0.16 \leq z \leq 0.36$ ). The thick solid line corresponds to the linear regression with the most probable parameters (see text). The confidence region ( $\beta = 1 - p = 0.998$ ), i.e. grey strip about the solid slant line, is also shown. The horizontal dashed line corresponds to the model  $n(D) = \text{const}$ . Results of  $\chi^2$ - (bottom left) and  $t$ -two-sided tests (bottom right) applied to assess a compatibility of the horizontal dashed line with the data are indicated in the insets. *Panel (d)*: Same as in the *panel (c)* but for brighter LOWZ galaxies ( $-23.2 \leq M_g \leq -22.2$ ).

the most probable parameters  $c_1 = 2.0 \times 10^{-4} (h^{-1} \text{ Mpc})^{-3}$  and  $c_2 = -1.8 \times 10^{-7} (h^{-1} \text{ Mpc})^{-4}$  for the *panel (c)*, and  $c_1 = 4.7 \times 10^{-5} (h^{-1} \text{ Mpc})^{-3}$  and  $c_2 = -1.5 \times 10^{-8} (h^{-1} \text{ Mpc})^{-4}$  for the *panel (d)*; in both cases  $\bar{D} = 745 h^{-1} \text{ Mpc}$ .

The horizontal dashed lines correspond to the conception of a volume-limited sample with nearly constant number density. Results of  $\chi^2$  and  $t$ -tests applied to assess a compatibility of these horizontal lines with the data on  $n(D)$  are shown in the insets at the bottom of both the panels (left and right, respectively). It can be seen that in the *panel (c)* the obtained values of  $\chi^2$  and  $t$  located far outside the confidence region at  $1 - p = 0.998$ .

On the other hand, the best fit in the *panel (c)* at  $M_g < -21.8$  gives the slant linear thick line that differs significantly from the horizontal dashed one. The confidence region at  $1 - p = 0.998$  about the linear dependence  $n(D)$  is also shown by narrow grey strip restricted by two dashed lines. Thus the hypothesis that  $n(D) =$

$\text{const}$  at  $M_g < -21.8$  does not statistically consistent with the set of  $n(D)$  values.

While, in the *panel (d)* at  $M_g < -22.2$  the solid thick line is in a good agreement with the horizontal dashed line, i.e. the number density of relatively brighter galaxies is close to homogeneous, which corresponds to the volume-limited sample. This means that the close-to-homogeneous distribution  $n(z)$  presented at  $M_g < -21.8$  in Fig. (2) by Kazin et al. (2010) is likely shifted for the LOWZ galaxies on absolute magnitude  $\Delta M_g \approx 0.4$  in accordance with Fig 4 (b), although such a shift occurs with a strong loss of statistics in the LOWZ catalog.

Fig. 5 shows the results of our model calculations reducing an influence of possible selection effects onto the inhomogeneous distribution  $n(D)$  of the DR12 LOWZ galaxies. For this purpose, many objects (points) are artificially added to each independent bin ( $\Delta_D = 10 h^{-1} \text{ Mpc}$ ) of comoving distances to get a uniform distribution at the level of the maximum value of  $n(D)$  in the



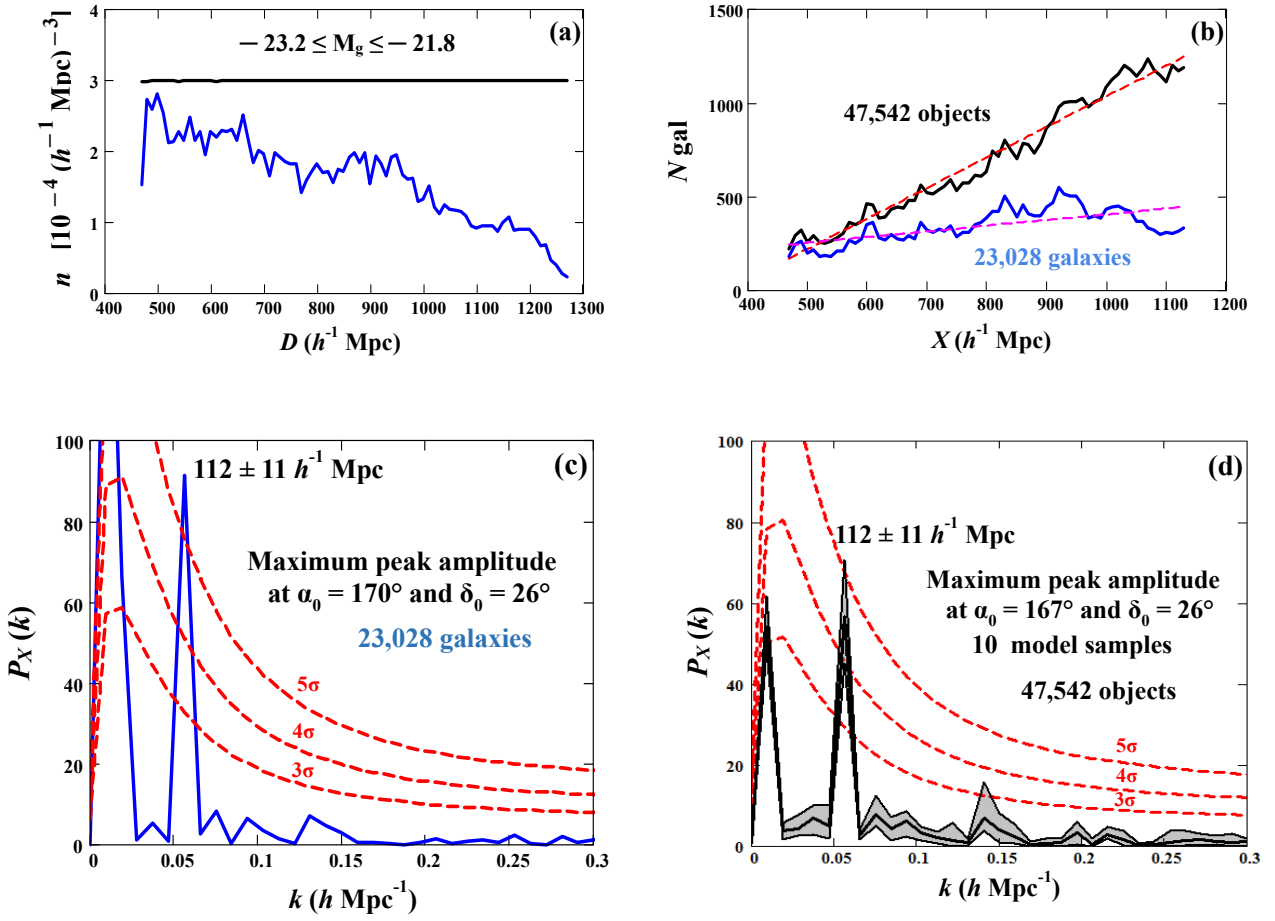


**Figure 5.** (Colour online) The results of modeling of the reduction of possible selection effects inherent to the statistics of LOWZ DR12 galaxies at  $-23.2 \leq M_g \leq -21.8$  and angular coordinates located within a smaller (light grey) rectangle ( $160^\circ \leq \alpha \leq 200^\circ$  and  $10^\circ \leq \delta \leq 46^\circ$ ) in Fig. 1 (see text). *Panel (a)*: the lower curve represents the number density of galaxies  $n(D)$  in units  $10^{-4} h^3 \text{Mpc}^{-3}$  as a function of the comoving distance  $D$  within the full interval under consideration  $464 \leq D(z) \leq 1274 h^{-1} \text{Mpc}$ ; upper horizontal line corresponds to the created sample of both the real galaxies and artificially added points randomly distributed in comoving space. *Panel (b)*: shows two distributions of projections of Cartesian coordinates on the  $X_0$ -axes within the fixed interval ( $464 \leq X \leq 1134 h^{-1} \text{Mpc}$ ); two  $X_0$ -axes are oriented in such a way that the dominant peak height of the power spectra at  $k = k_{\text{max}} = 0.056 h \text{Mpc}^{-1}$  calculated separately for the sample of 23,028 galaxies and the model sample of 47,542 objects would be maximum; two directions of  $X_0$  (i.e.  $\alpha_0$  and  $\delta_0$ ) are indicated in the *panels (c)* and *(d)*, respectively. The lower curve corresponds to the sample of galaxies, while the upper rising curve is an example of model sample; dashed lines depict linear trends of the two distributions. *Panel (c)*: shows the 1D power spectrum calculated for the projections of Cartesian coordinates of real galaxies on the  $X_0$ -axis. *Panel (d)*: plots the 1D power spectrum (thick black line) averaged over 10 power spectra calculated for randomly selected model samples and a variations of peak amplitudes (at  $0 \leq k \leq 0.3$ ) corresponding to the same 10 model power spectra (grey strip bounded by two thin lines). Dashed lines in *panels (c)* and *(d)* indicate significance levels calculated in the same manner as the dashed lines in the *right panels* of Figs. 2 and 3 (see text).

considered range  $D$ . Objects (points) are added to each bin  $\Delta D$  randomly, so that the two angular coordinates  $\alpha$  and  $\delta$  as well as the comoving distance itself, correspond to uniform distribution (Poisson's distribution in space). Joint distribution of these added objects and real LOWZ galaxies forms a model sample, represented by the horizontal line in the *panel (a)*.

The properties of the spatial distribution corresponding to the total model sample can be examined using the procedure outlined in Sect. 3 but with some variations. To do this, as in Sects. 4 and 5, a Cartesian coordinate system is introduced, which rotates in such a way that the  $X$ -axis scans with a step of  $1^\circ$  over the entire area outlined by the dotted line in Fig. 1, i.e. the same area as it is used in Figs. 2 and 3. For each  $X$ -direction, projections of the coordinates of both artificial and real galaxies (model sample) onto this axis are produced, then 1D normalized distribution and its power spectrum

are calculated. For comparison all subsequent calculations are also carried out separately for real LOWZ galaxies within the same range of values  $M_g$ ,  $\alpha$ ,  $\delta$  and  $X$ .

It should be noted that for the model sample it is not possible to coherently construct a normalized 1D distribution function using Eq. (3) and calculate the power spectrum using Eq. (4) for the entire interval  $464 \leq X \leq 1274 h^{-1} \text{Mpc}$ . This is a consequence of a complex trend of the dependence  $N_X(X)$  having a rather high maximum at  $X \sim 1100 h^{-1} \text{Mpc}$  and a sharp subsequent decline (not shown in Fig. 5 (b)). Therefore, we have to decrease the interval  $X$  up to  $464 \leq X \leq 1134 h^{-1} \text{Mpc}$ , so that the distribution of the model sample well described (using the least squares method) by the simplest linear trend, which is shown in Fig. 5 (b). Replacing in Eq. (3) the mean value  $S_X$  by a linear trend  $N_L(X) = s_1 + s_2 X$ , where  $s_1$  and  $s_2$  are determined constants, and using formula Eq. (4),

we obtain the power spectra for both the sample of LOWZ galaxies Fig. 5 (c) and the model sample Fig. 5 (d).

Fig. 5 (c) represents the power spectrum of 1D distribution  $NN(X)$  of real galaxies with limited absolute magnitudes ( $-23.2 \leq M_g \leq -21.8$ ) in the direction  $X_0$  of the maximum peak. The spectrum plotted using the linear trend [shown at the bottom of Fig. 5 (b)]. We see that the significance of this peak exceeds  $5\sigma$ .

Fig. 5 (d) demonstrates the results of power spectra calculations carried out for 10 model samples using the same algorithm as described above. Various realizations of power spectra form a strip of variations (light grey) visible in the panel. This strip, at  $k = k_{\max} = 0.056$  corresponds to the scatter of peaks whose amplitudes lie in the interval of significance from  $4\sigma$  to  $5\sigma$ . There are also shown the power spectrum averaged over all 10 realizations. The  $X_0$ -direction indicated in the panel (d) corresponds to the highest peak amplitude among all 10 realizations. Note that Fig. 5 (b) plots the  $N_X(X)$  distribution for the same direction.

Significance levels in Figs. 5 (c) and (d) were carried out according to the same procedure as described above for the significance levels in Figs. 2 and 3, i.e. using the same area of  $X$ -directions ( $180^\circ \leq \alpha \leq 200^\circ$  and  $20^\circ \leq \delta \leq 40^\circ$ ), in which there are no significant peaks in the power spectra. Note also a slight shift of peak centers in both the power spectra relative to the position of peaks in Figs. 2 and 3 but quite consistent with them. The shift possibly related to the use of the linear trend  $N_L(X)$  instead of the mean value  $S_X$  in the modification of Eq. (3).

Thus, the model calculations carried out here show that the artificial intrusion of random objects, which ensures the homogeneous number density  $n(z)$  of the model sample, does not smooth out the quasi-periodic feature in the spatial distribution of galaxies. In other words, we are dealing with a rather robust quasi-periodicity.

## 7 CONCLUSIONS AND DISCUSSION

In this work on the base of SDSS DR12 LOWZ catalogue we study possible large-scale quasi-regular structure in the spatial distribution of cosmologically distant galaxies at redshifts  $0.16 \leq z \leq 0.47$ , or comoving distances  $464 \leq D \leq 1274 h^{-1}$  Mpc.

Unlike our previous papers (e.g. Ryabinkov & Kaminker 2014, Paper I, Paper II), here we do not consider the radial distributions of objects in space but use others, as it turned out to be more sensitive, methods of registration of possible quasi-regular structures located at cosmological distances. We apply the method proposed in Paper II of projecting the Cartesian coordinates of galaxies onto different  $X$ -axes sequentially rotated within definite region on the sky.

We use two modifications of projections in each rotational state of the  $X$ -axis, namely, (i) the projections onto the  $X$ -axes of the Cartesian coordinates of all galaxies located in the definite interval  $z_1 \leq z \leq z_2$  and detected within a certain region in the sky (light grey rectangle in Fig. 1), (ii) similar projections on the  $X$ -axis of coordinates of all galaxies falling into the imaginary rotating *cuboid* whose faces (edges and vertices) are defined in the  $XYZ$ -coordinate system rigidly connected with the cuboid. When rotating, the cuboid captures unlike the case (i) different samples of the LOWZ galaxies located mainly within the large rectangle in Fig. 1. In each rotational state we calculate 1D distribution of the projections of galaxy coordinates (captured in this way) onto the  $X$  axis with a fixed interval  $X_1 \leq X \leq X_2$ .

In both the cases we plot the normalized 1D distributions along each  $X$ -axis and calculate the corresponding power spectrum. Thus,

the direction of the maximum peak heights  $X_0$  ( $\alpha_0, \delta_0$ ) of the power spectrum in a narrow range  $0.05 < k < 0.07$  can be found among a set of directions  $X$  with various power spectra. In the case (i) we perform the so-called discrete 3D Radon transform along a given  $X$ -axis and calculate its power spectrum, keeping in mind that the real direction of quasi-periodicity can be parallel to the found axis  $X_0$  but arbitrary shifted in space. While in the case (ii) we have a chance at least roughly to localize this structure in space.

To make assessments of significance we use an approach of exponential probability [see Eq. (5)] to get a value of randomly distributed peak heights in the power spectra. The key of such assessment is calculation of the average power spectrum  $\langle P(k) \rangle$  with variable variance throughout the whole region,  $0.0 < k \leq 0.3$ , under consideration. These spectra were averaged over the “background” region in the sky ( $180^\circ \leq \alpha \leq 200^\circ$  and  $20^\circ \leq \delta \leq 40^\circ$  – a half of the scanning area outlined by the dotted line in Fig. 1) in which there are no significant peaks in the power spectrum.

Using the set of recipes presented above, we get the following results:

1. In all cases considered in Figs. 2, 3 and 5(c) we got the same significant periods  $116 \pm 10 h^{-1}$  Mpc as in Paper II, which used the data on LRGs of the SDSS DR7 and preliminary exploited the data on galaxies of the DR12.
2. The special  $X_0$  - directions considered in this paper as well as in Paper II locate within a compact region in the sky  $\alpha_0 \simeq 172^\circ \pm 5^\circ$  and  $\delta_0 \simeq 26^\circ \pm 2^\circ$ .
3. In the case of a rotating cuboid, when it gradually captures the large number of galaxies in different phases of rotation, we get the highest significance peak ( $\gtrsim 5\sigma$ ) corresponding to the same period  $116 \pm 10 h^{-1}$  Mpc and the same maximum-peak direction  $X_0$  as in the cases of the Radon projections.
4. The distribution of the number density of relatively bright LOWZ galaxies at the absolute  $g$ -band magnitude  $M_g \leq -21.8$ , lying within the large rectangle in Fig. 1, is not homogeneous relative to the comoving distances  $D \lesssim 1000 h^{-1}$  Mpc ( $z \lesssim 0.36$ ), but rather corresponds to a linear regression, i.e. strictly speaking it is not the volume-limited sample. The number density approaches to homogeneous one only for the brightest and rarest objects  $M_g \leq -22.2$  for which the statistics are small.
5. The peaks in the power spectra of 1D distributions of the projections of the Cartesian coordinates of galaxies on the special  $X_0$ -axis turn out to be resistant to the replenishment by a large number of random points (artificial galaxies) in order to reach the homogeneous total number density. The position of the peaks shifts somewhat (within errors), and their high significance is retained.
6. The estimations produced for the sample of LOWZ galaxies providing projections onto the  $X_0$  direction in Fig. 2 show that a signal-to-noise ratio for the major spatial harmonic (at  $k = k_{\max}$ ) is  $\gtrsim 3.0$ , then the contrast of 1D density projections of coordinates of galaxies  $N_X(X)$  corresponding to the same harmonic can be estimated as  $\gtrsim 0.1$ .<sup>12</sup> Worth to note that these characteristics were obtained only when applying the method of projections onto the

<sup>12</sup> Following Paper II, we use a modification of Eqs. (6), (7) and (9) of Scargle (1982), which we separately tested with simulations. It allows to estimate the amplitude of the fundamental harmonic  $A(k_{\max})$  included in the signal-to-noise ratio (Eq. 3), i.e.  $\langle S/N \rangle(k_{\max}) = A(k_{\max}) \gtrsim \langle \sqrt{4P(k_{\max})/N_b} \rangle$ , where  $P(k_{\max})$  is a height of the main peaks in the power spectra,  $N_b$  is a number of bins accepted in each direction  $X$ ,  $\langle \dots \rangle$  is averaging over all bins along  $X_0$ -axis. Then 1D density contrast corresponding to the fundamental harmonic is  $\delta(k_{\max}) \gtrsim \sqrt{4P(k_{\max})/N_G}$ , where  $N_G = N_b \cdot S_X$  is a full number of

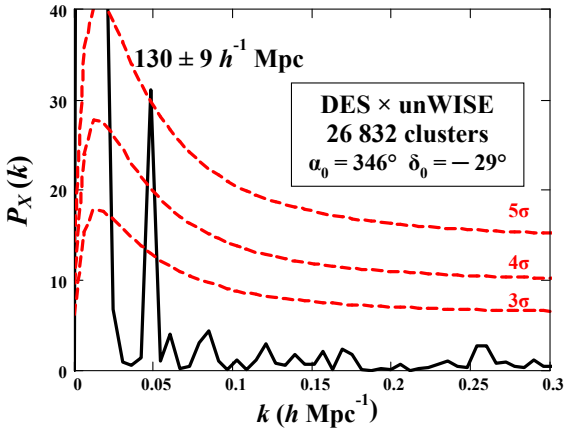


**Figure 6.** (Colour online) 1D power spectrum  $P_X(k)$  (solid curve), calculated for the distribution of projections of the Cartesian coordinates of galaxy clusters on the  $X_0$ -axis corresponding to maximum peak height at  $0.04 < k_{\max} < 0.06 h \text{ Mpc}^{-1}$  (similar to the right panel in Fig. 2). The spectrum was calculated for an array of clusters from the catalog DES×unWISE with  $z$  determined from photometric data with accuracy  $\delta z \lesssim 0.013$ . Dashed curves are drawn according to the significance levels of the peaks ( $3\sigma$ ,  $4\sigma$ , and  $5\sigma$ , respectively) extended to the entire considered range of  $k$ ; the maximum peak corresponds to  $k_{\max} = 0.048 \pm 0.004 h \text{ Mpc}^{-1}$ .

$X$  axis, i.e. essentially an integral method that collects information from a large amount of galaxies scattered over the space. In reality, we are dealing with an extremely weak and shallow ripples in the spatial distribution of galaxies, in contrast to much more prominent quasi-regular formations found in the spatial distribution of galaxy superclusters at  $z \lesssim 0.13$  (e.g. Einasto et al. 1997d, Einasto et al. 1997b, Einasto 2014, Saar et al. 2002).

All conclusions of this work, made so far, are obtained on the basis of a statistical analysis of the spectroscopic measurement of redshifts  $z$ , at which the accuracy of determination  $z < 0.5$  is approximately  $\delta z \approx 4 \times 10^{-4}$  (e.g. Bolton et al. 2012). This is quite sufficient accuracy to identify the average period  $\Delta z \sim 0.04$  over the entire interval  $z$ . However, over the past decades such statistical methods have appeared, associated with huge amounts of data, which have made it possible to significantly refine the photometric measurements of  $z$  (e.g. De Vicente et al. 2016 and references therein) for both galaxies and clusters of galaxies, the latter with greater accuracy (e.g. Wen & Han 2021, 2022).

Trying to expand the scope of the search we carried out a series of very preliminary calculations to study the spatial distributions of galaxy clusters with a relatively accurate definition of photometric  $z$  (results will be published elsewhere). In particular, we analyzed the spatial distribution of clusters, located in the southern part of the sky, based on the catalog, presented by Wen & Han (2022). The uncertainty of the cluster redshifts  $z$  is  $\lesssim 0.013$ , which is quite sufficient to identify the quasi-periodicity pertaining to the peaks in the power spectra at  $0.04 < k_{\max} < 0.06$ . The interval is slightly shifted with respect to the LOWZ spectroscopic data analysis.

We have applied the technique described in Sects. 3 and 4 to carry out analysis of 26, 832 clusters from the catalog,<sup>13</sup> (file:

projections of coordinates onto the  $X_0$  axis,  $S_X$  is the average number of the projections per a bin.

<sup>13</sup> [http://zmtt.bao.ac.cn/galaxy\\_clusters/catalogs.html](http://zmtt.bao.ac.cn/galaxy_clusters/catalogs.html)

cluster\_DESunWISE.dat.gz) with photometric  $z$  belonging to an interval  $0.1 \leq z \leq 0.47$ .

Based on this statistics we built the Radon transforms and using Eq. (4) calculated the power spectra of 1D distributions of projections of cluster coordinates on the  $X$ -axes with different orientations, but at fixed interval  $132 \leq X \leq 1172 h^{-1} \text{ Mpc}$  ( $0.1 \leq z \leq 0.47$ ). Directions of  $X$ -axis were changed within an angular area  $340^\circ \leq \alpha \leq 360^\circ$ ,  $-40^\circ \leq \delta \leq -20^\circ$  with a step by one degree. The same region of angular scanning with the  $X$ -axis was used in order to calculate the significance levels for all considered  $k$  ( $0 < k < 0.3 h \text{ Mpc}^{-1}$ ).

Fig. 6 shows the preliminary results of such calculations. One can see a significant dominant peak at  $k = 0.048 \pm 0.004 h \text{ Mpc}^{-1}$  (period  $130 \pm 9 h^{-1} \text{ Mpc}$ ) in the 1D power spectrum corresponding to the  $X_0$  direction with angular coordinates  $\alpha_0 \simeq 346^\circ$  and  $\delta_0 \simeq -29^\circ$ . Significance of the peak exceeded  $5\sigma$ .

Thus the indicated direction is approximately a continuation of the selected direction in the northern hemisphere (see above), which is reminiscent of the results by Broadhurst et al. (1990), Szalay et al. (1993), Koo et al. (1993) (see discussion in Paper II). Although the selected bundle of close directions (with high level of significance of the peaks) is somewhat rotated (by  $\sim 20^\circ - 30^\circ$ ) in right ascension  $\alpha$  relative to the axis connecting the north and south galactic poles ( $\alpha_{\text{ngp}} = 192.85^\circ$ ,  $\alpha_{\text{sgp}} = 12.85^\circ$  ( $372.85^\circ$ )). In the same time the declinations  $\delta$  are close the declinations of northern ( $\delta_{\text{ngp}} = 27.13^\circ$ ) and southern ( $\delta_{\text{sgp}} = -27.13^\circ$ ) poles, respectively. Consequently, we got preliminary sketches of weak large-scale anisotropy in the distribution of galaxies(north) and clusters(south), which may have a dipole character with slightly different features in the north and south sky. This fact in itself requires careful verification and further confirmation.

Let us note, that some small discrepancy between north and south data was found recently by calculations of the Minkowski functionals (Appleby et al. 2022) on the basis of the LOWZ statistics. These results do not contradict to the assumption of the anisotropy of the spatial distribution of matter (emphasized by the authors), as well as the assumption about large scale inhomogeneity of the distribution, since the data of the LOWZ cover a limited domain of space. While the calculations based on the CMASS data (corresponding to larger redshifts) no longer show north/south discrepancy (see Appleby et al. 2022 for details).

Thus the present study confirms the hypothesis formulated in Paper II that at the redshifts considered here, there may be a huge elongated quasi-periodic structure that represents an alternation of flat condensation and rarefaction of matter with a characteristic scale  $\Delta X = 116 \pm 10 h^{-1} \text{ Mpc}$ . Along the directions close to that found in this work the structure is likely to have a total scale  $\gtrsim 800 h^{-1} \text{ Mpc}$ . In other words we find traces of two scales of an anisotropic quasi-regular structure the quasi-period pointed out above and entire scale, on which this period appears. At the same time, the very existence of such a structure remains a hypothesis requiring further confirmation.

## ACKNOWLEDGMENTS

We are extremely grateful to an anonymous reviewer for his numerous and very helpful comments.

**DATA AVAILABILITY**

[dataset]\* Reid B. et al., 2016, Large-scale structure catalogues, galaxy\_DR12v5\_LOWZ\_North.fits.gz, galaxy\_DR12v5\_CMASSLOWZE3\_North.fits.gz, galaxy\_DR12v5\_CMASS\_North.fits.gz, <https://data.sdss3.org/sas/dr12/boss/lss/>

[dataset]\* Beck R. et al., 2016, SDSS SkyServer, Sample SQL Queries, <http://skyserver.sdss.org/dr12/en/help/docs/realquery.aspx>

[dataset]\* Kazin E.A. et al., 2010, Sloan-digital sky survey LRG sample, Full DR7 LRG sample (data ascii), <https://cosmo.nyu.edu/~eak306/SDSS-LRG.html>

[dataset]\* Wen Z.L., Han J.L., 2022, Catalogs of clusters of galaxies, cluster\_DESunWISE.dat.gz, [http://zmtt.bao.ac.cn/galaxy\\_clusters/catalogs.html](http://zmtt.bao.ac.cn/galaxy_clusters/catalogs.html)

**References**

Alam S., et al., 2015, *ApJS*, 219, 12  
 Appleby S., Park C., Pranav P., Hong S. E., Hwang H. S., Kim J., Buchert T., 2022, *ApJ*, 928, 108  
 Bardeen J. M., Bond J. R., Kaiser N., Szalay A. S., 1986, *ApJ*, 304, 15  
 Beck R., Dobos L., Budavári T., Szalay A. S., Csabai I., 2016, *MNRAS*, 460, 1371  
 Bolton A. S., et al., 2012, *AJ*, 144, 144  
 Broadhurst T. J., Ellis R. S., Koo D. C., Szalay A. S., 1990, *Nature*, 343, 726  
 Dawson K. S., et al., 2013, *AJ*, 145, 10  
 De Vicente J., Sánchez E., Sevilla-Noarbe I., 2016, *MNRAS*, 459, 3078  
 Deans S. R., 2007, *The Radon transform and some of its applications*. New York, Dover Publications., Inc.  
 Einasto J., 2014, *Dark Matter and Cosmic Web Story*. World Scientific  
 Einasto M., Einasto J., Tago E., Dalton G. B., Andernach H., 1994, *MNRAS*, 269, 301  
 Einasto M., Tago E., Jaaniste J., Einasto J., Andernach H., 1997a, *A&AS*, 123, 119  
 Einasto J., et al., 1997b, *MNRAS*, 289, 801  
 Einasto J., Einasto M., Frisch P., Gottlober S., Muller V., Saar V., Starobinsky A. A., Tucker D., 1997c, *MNRAS*, 289, 813  
 Einasto J., et al., 1997d, *Nature*, 385, 139  
 Einasto J., et al., 2011a, *A&A*, 531, A75  
 Einasto J., et al., 2011b, *A&A*, 534, A128  
 Einasto M., et al., 2016, *Astron. Astrophys.*, 587, A116  
 Einasto J., Suhhonenko I., Liivamägi L. J., Einasto M., 2019, *A&A*, 623, A97  
 Feldman H. A., Kaiser N., Peacock J. A., 1994, *ApJ*, 426, 23  
 Hogg D. W., 1999, astro-ph/9905116  
 Kaiser N., Peacock J. A., 1991, *ApJ*, 379, 482  
 Kayser R., Helbig P., Schramm T., 1997, *Astron. Astrophys.*, 318  
 Kazin E. A., et al., 2010, *ApJ*, 710, 1444  
 Kerscher M., 1998, *A&A*, 336, 29  
 Kerscher M., 2000, in Mecker K. R., Stoyan D., eds, *Lecture Notes in Physics* Vol. 554, *Statistical Physics and Spatial Statistics*. Berlin Springer Verlag, pp 36–71  
 Kerscher M., et al., 1997, *MNRAS*, 284, 73  
 Koo D. C., Ellman N., Kron R. G., Munn J. A., Szalay A. S., Broadhursts T. J., Ellis R. S., 1993, in Chincarini G. L., Iovino A., Maccacaro T., Maccagni D., eds, *Astronomical Society of the Pacific Conference Series* Vol. 51, *Observational Cosmology*. p. 112  
 Landy S. D., Shectman S. A., Lin H., Kirshner R. P., Oemler A. A., Tucker D., 1996, *ApJ*, 456, L1

Ledermann W., Lloyd E., 1984, *Handbook of Applicable Mathematics*. Vol. VI: Statistics. John Wiley & Sons, New York  
 Mecke K. R., 2000, in Mecker K. R., Stoyan D., eds, *Lecture Notes in Physics* Vol. 554, *Statistical Physics and Spatial Statistics*. Berlin Springer Verlag, pp 111–184  
 Reid B., et al., 2016, *MNRAS*, 455, 1553  
 Ryabinkov A. I., Kaminker A. D., 2014, *MNRAS*, 440, 2388  
 Ryabinkov A. I., Kaminker A. D., 2019, *Ap&SS*, 364, 129 (Paper I)  
 Ryabinkov A. I., Kaminker A. D., 2021, *Universe*, 7, 289 (Paper II)  
 Ryabinkov A. I., Kurov A. A., Kaminker A. D., 2013, *Ap&SS*, 344, 219  
 Saar E., Einasto J., Toomet O., Starobinsky A. A., Andernach H., Einasto M., Kasak E., Tago E., 2002, *A&A*, 393, 1  
 Sahni V., Sathyaprakash B. S., Shandarin S. F., 1998, *ApJ*, 495, L5  
 Scargle J. D., 1982, *ApJ*, 263, 835  
 Starck J. L., Martínez V. J., Donoho D. L., Levi O., Querre P., Saar E., 2005, *EURASIP Journal on Applied Signal Processing*, p. 483071  
 Szalay A. S., Ellis R. S., Koo D. C., Broadhurst T. J., 1991, in Holt S. S., Bennett C. L., Trimble V., eds, *American Institute of Physics Conference Series* Vol. 222, *After the first three minutes*. p. 261  
 Szalay A. S., Broadhurst T. J., Ellman N., Koo D. C., Ellis R. S., 1993, *Proc. Natl. Acad. Sci. USA*, 90, 4853  
 Wen Z. L., Han J. L., 2021, *MNRAS*, 500, 1003  
 Wen Z. L., Han J. L., 2022, *MNRAS*, 513, 3946  
 Wen Z. L., Han J. L., Liu F. S., 2012, *ApJS*, 199, 34  
 Yoshida N., et al., 2001, *MNRAS*, 325, 803  
 van de Weygaert R., 2016, in van de Weygaert R., Shandarin S., Saar E., Einasto J., eds, *IAU Symposium* Vol. 308, *The Zeldovich Universe: Genesis and Growth of the Cosmic Web*. pp 493–523  
 van de Weygaert R., Schaap W., 2009, in Martínez V. J., Saar E., Martínez-González E., Pons-Bordería M. J., eds, *Lecture Notes in Physics* Vol. 665, *Data Analysis in Cosmology*. Berlin Springer Verlag, pp 291–413